Measurements and modelling of molecular diffusion of glycerol solutions through the Wiener optical method and image analysis

Jochem Langen
L2 Research Led Investigation, Group H1, Lab partner: Rebecca Graydon
Submitted: 26-07-2022; Dates of Experiment: week 8-11 2021

In this work, a method is detailed to measure molecular diffusion using the Wiener optical method described with the home-environment in mind. To this end, the length of the dip and the full width half maximum (fwhm) will be determined. This will be done through image analysis, the process of which is described. Additionally, a computational model of the optical effect is presented, which can be compared to obtained data.

I Introduction

The Wiener optical method [1] of measuring molecular diffusion is based on the principle that the diffusing liquids have different refractive indices n. As these liquids mix, the composition of n throughout the entire body of water changes as well as the gradient in n. The refractive index and its gradient affect the path of light travelling through a container with two diffusing liquids stacked on top of one-another. This causes a dip to form in the laser pattern observed. From the shape of this dip, one could infer properties of the molecular diffusion effect.

I.1 Molecular Diffusion

Disregarding the effect gravity plays on the molecular diffusion, the diffusion of a concentration in a medium can be considered by Fick's second law [1], which is the following parabolic equation:

$$\frac{\partial c}{\partial t} = D\frac{\partial^2 c}{\partial z^2}, \tag{1}$$

where c is the mass concentration of glycerol, t is time, D is the diffusion coefficient and z is the height in the container; D is assumed to be independent of c. As the two liquids are poured on top of one-another we have the following initial condition:

$$0 \leq z < h : c(z,0) = c_0 \;\&\; h < z \leq L : c(z,0) = 0, \tag{2}$$

where h is the height of the interface between the two liquids, L the total height of the fluid column and c_0 the concentration of glycerol in the bottom solution. As no concentration can flow through the bottom of the container nor is approximately not dissipated through the air, the system has the following boundary conditions:

$$\frac{\partial c(0,t)}{\partial z} = 0 \;\&\; \frac{\partial c(L,t)}{\partial z} = 0. \tag{3}$$

This PDE can be solved using Separation of Variables to give:

$$c(z,t) = c_0\left(\frac{1}{2} + \sum_{n=1}^{\infty} \frac{2}{n\pi} sin\left(\frac{n\pi}{2}\right) cos\left(\frac{n\pi z}{L}\right) exp\left(-\frac{n^2\pi^2 D}{L^2}t\right)\right). \tag{4}$$

The z-derivative c_z of this equation has been determined to be:

$$c_z(z,t) = -c_0 \sum_{n=1}^{\infty} \frac{2}{L} sin\left(\frac{n\pi}{2}\right) sin\left(\frac{n\pi z}{L}\right) exp\left(-\frac{n^2\pi^2 D}{L^2}t\right)\right). \tag{5}$$

An example of these two results have been plotted in Fig. 1 for the parameters of one of the experiments.

I.2 Ray-tracing

To determine how the light diffracted by the solution behaves, we can use geometric optics for which we use the eikonal equation inside the container; where the curvature of the light ray is defined as [2]

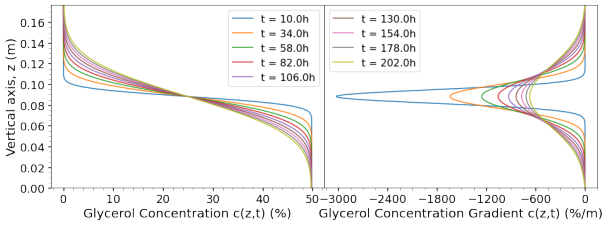

Figure 1: The glycerol concentration and its gradient in % & %/m respectively. The model is shown for $L = 17.65\,cm$, $D = 6e-10\,m^2s^{-1}$ and $c0 = 49.85\%$.

$$n\vec{\mathbf{K}} = \boldsymbol{\nabla} n - \vec{\mathbf{s}}(\vec{\mathbf{s}} \bullet \boldsymbol{\nabla} n), \tag{6}$$

where n is the refractive index (not to be confused with the summation index as seen in eq. 4 & 5), $\vec{\mathbf{K}}$ the curvature of the light ray, $\vec{\mathbf{s}}$ the unit direction vector and $\boldsymbol{\nabla}$ the del operator. Here, $n\vec{\mathbf{K}}$ represents the part of spatial derivative of n that is perpendicular to the light ray direction of propagation. If we assume n to change linearly with the concentration of glycerol then we can define it as follows:

$$n = n_w + \frac{c(z,t)}{c_G}(n_G - n_w), \tag{7}$$

where n_w & n_G are the refractive indices of water and a glycerol solution with concentration c_G respectively. As the refractive is approximated to be constant along the x y axis, we can use eq. 5 plugged into the derivative of eq. 7 for $\boldsymbol{\nabla} n$. In this way eq. 6 becomes a 2nd order PDE but only with z-dependence for the highest order. This equation was solved essentially using the Euler-Cromer method, but extended to 3-dimensions.

Instead of evaluating the c & c_z every time $\boldsymbol{\nabla} n$ is, an array is created in advance containing these parameters for a large list of z-values. When determining $\boldsymbol{\nabla} n$ the values for c & c_z are used which have a z-value closest to that of the light ray in the model. The container is essentially split up into many sections and an evaluation is done to see what section the light ray is currently in.

II Methods

II.1 Experiment

II.1.1 The Set-up

The experimental set-up consists of a laser, glass rod, container with the two liquids, a thermometer and a screen with reference lines to use in the image analysis; this set-up is displayed in Fig. 2. The glass rod is used as a cylindrical lens and spreads out the approximately non-diverging laser beam into a fan. This is done to create a thin beam slicing at least the entire back-side of the container, going through each level of the liquid mixture. A small focal length of this

Jochem Langen

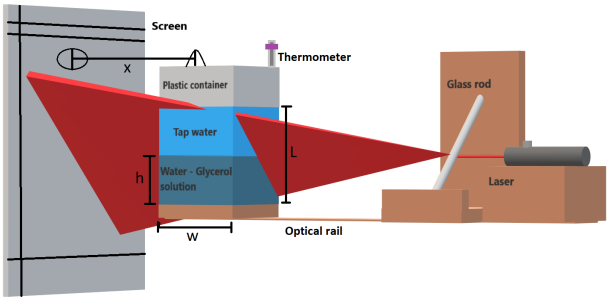

Figure 2: A 3D representation of the Experimental set-up. The components are annotated as well as some dimensions of interest: x, h, L & w. The coloured parts of the rectangular shape denote the different liquids held inside with an exception of the brown part on the bottom, which represents the cardboard stand as throughout the image. The screen shows the black reference lines. The red rectangular shape coming from the glass rod depicts the laser as it travels through the set-up.

diverging cylindrical lens is preferred as this will increase the ray convergence and consequently the spread of the fan past the focal length; hence reducing the distance required for the fan to reach the size of the diagonal of the side of the part of the container with liquid. The focal length f for a cylindrical lens is determined as follows:

$$f = \frac{nR}{2(n-1)}, \tag{8}$$

where n is the refractive index as before and R is the lens radius, this is derived from the lens makers' equation. A balance between the benefit of a smaller optical rail and ease of setting the laser up to hit the approximate centre of the glass rod resulted in a 7 mm rod radius. As the rod spreads the laser perpendicularly the angle at which it needs to be inserted α_{rod} in its stand is given by:

$$\alpha_{rod} = tan^{-1}(\frac{L}{w}). \tag{9}$$

A plastic container with a maximised height is used to increase the time for which the analytical solutions to the molecular diffusion are valid [1]. In determining the additional liquid to use, next to tap water its density, viscosity, solubility and refractive index were considered. The bigger the density viscosity is of one liquid compared to the other the better the stacking of liquids will go as the lighter, more fluid liquid will spread more easily on the top without diffusing with the one below. Additionally, a larger refractive index difference will increase the optical effect. Glycerol was used as a fluid to provide a comparison with existing literature [1] and also adhere relatively good to the aforementioned. The denser glycerol solution is put in the bottom as this will cause gravity to only affect the molecular diffusion by potentially slowing it down, dragging the glycerol back down but it will not cause further diffusion itself.

In positioning the container relative to the screen, a balance is sought between the larger distance causing the laser beam to spread out more in width (due to beamwidth) and fan front, reducing its brightness and increasing the spread of the beam, making the image analysis harder and less accurate; and the shorter distance making for a larger angle of the image relative to the normal to the screen, distorting the image. This image was taken from the side of the optical rail, next to the side of the container facing the screen.

Horizontal and vertical dark lines are drawn on the screen to provide known references for the image analysis.

Particularly due to the at-home nature of the experiment, a low class (2) laser was used and an obscuring structure was built around it to prevent potential eye strain. A thermometer has been used to measure the liquid temperature in order to determine the refractive indices used in the ray-tracing model. Cardboard, duct tape blu-tack were used to build the set-up due to their availability and ease of use.

II.1.2 Experimental procedure

The fluids had been stacked by pouring the lighter liquid onto a spoon inserted at the top of the fluid surface. As the interface between the two liquids is halfway between them, consequent experiments can be run with half the initial concentration by mixing the previous mixture. A photo was taken as soon as the pouring was finished with further images taken every 5 minutes thereafter. The interval between subsequent images was increased over time as the change in laser pattern was expected to follow a inverse square-root relationship [1]. As a notable laser pattern could be observed for a long time after the start of the experiment, data-sets were taken spanning up to 8 days. The dimensions of all the components, and of the distances between them as well as a fixed reference point (wall) were measured using a ruler and tape measure, after every experiment run.

II.2 Image analysis

The images were analysed using Python in Jupyter Notebook, particularly making use of the OpenCV library [2]. The aim of this programme would be to autonomously transform the image to account for its perspective and extract the laser dip length and fwhm.

II.2.1 Image Transformation

The OpenCV "getPerspectiveTransform" & "warpPerspective" [2] functions were utilised to obtain a 3x3 transformation matrix and apply this to all the coordinates respectively. Four points on the original image and transformed image are needed to generate this matrix, for which a point recognition algorithm has been written. These points must form a rectangular shape, where the more the shape fills the image, the better the transform will be. This is because points closer together will amplify inaccuracies in their recognition, skewing the transformed image. An example of a transformed image is shown in Fig. 3.

II.2.2 Hough Line Transform

To extract the right reference points, the reference lines need to be detected on the image for which Hough Line transformations were used. This process is built up out of three steps, firstly greyscaling the image, then extracting the recognised edges on the image and finally using these edges to fit lines to them. The edge detection was done through the OpenCV "Canny" [2] function, for which intensity gradient limits are provided; an upper limit above which the points are definite edges and a lower limit, the area between which defines points as edges dependent on connectivity with other edges. The Hough Line transform creates lines defined by a ρ & θ value, defined as the shortest distance between the line and the top left corner of the image and the corresponding angle clockwise down from the horizontal; with $0 \leq \theta \leq \pi$ and ρ that can be positive and negative.

These lines are compared with the pixels with RGB values below a defined intensity threshold to extract the pixels on the images corresponding to these dark lines. The outermost pixels in that range (along the x- & y-axis) provide the line endpoints, the reference points used.
Additionally, the lines fitted to the laser pattern are used to discard laser artefacts scattered across the image (not part of the line nor dip), as only the pixels close (line) and below (dip) are utilised. An example of these lines can be seen in Fig. 3.

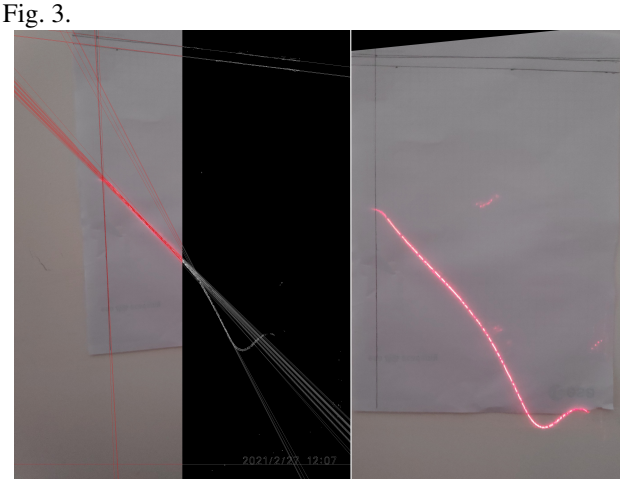

Figure 3: An image of the 50-50 glycerol-water solution $L = 10.7\,cm$ data set taken at $t = 8.837 \pm 0.012e4\,s$. The part on the left shows the image as taken on the LHS and the extracted edges on the RHS, both with the Hough Lines overlayed in red and white; the part on the right shows the resultant transformed image.

III Results

Four data sets have been analysed, with differing concentrations and/or water levels. The data obtained is plotted in Fig. 4 & 5. As the laser utilised has a wavelength between 640 nm & 660 nm a range for n_W was used of 1.330238 to 1.331144 [3], giving $n_w = 1.3307 \pm 0.0009$. The values used for glycerol can be found in table 1.

Data set:	Black	Green	Blue	Red
Glycerol concentration, $c_0\ (mass\%)$	49.9 ± 0.1	99.7 ± 0.1	74.8 ± 0.1	49.9 ± 0.1
Refractive index, n_G	1.3081 ± 0.0015	1.4740 ± 0.0016	1.4353 ± 0.0015	1.3081 ± 0.0015
Water level, $L\ (m)$	0.1070 ± 0.0004	0.1080 ± 0.0004	0.177 ± 0.005	0.1765 ± 0.0004

Table 1: The initial concentrations and refractive indices of the glycerol solutions used. These indices are determined at 20°C and go up by 0.000225 per 1°C

From the data in Fig. 4 it can be observed at early time the data is on a horizontal linear regime w.r.t. $1/sqrt(t)$ whilst it later converges to a more vertical linear regime. The latter can be concluded with more certainty as the density of the data there is much higher and the errors smaller. This agrees with results found in other literature [1]. Additionally, all the data sets appear to converge to the same vertical line. Though the Black data set appears to have a few outliers when compared to the general shape in the other data sets, the Black and Red data appear to follow the same shape. Though it is these outliers that make for no decisive conclusion on whether the height of the water column has an effect on the dip length.
From the data in Fig. 5 it can be observed that the data sets with a smaller water level (Black & Green) have a much steeper increase in fwhm but the longer Green data set reaches a plateau early, whilst the other data (Blue & Red) show a much more shallow increase which then also does not flatten as quickly. Observing the images themselves, it

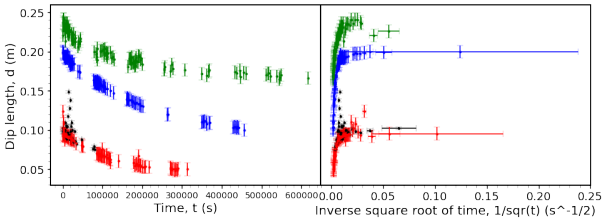

Figure 4: The length of the dip in the laser pattern compared to the height of the liquid interface from the data sets as described in table 1. It is plotted against time on the LHS and the inverse square root of time on the RHS.

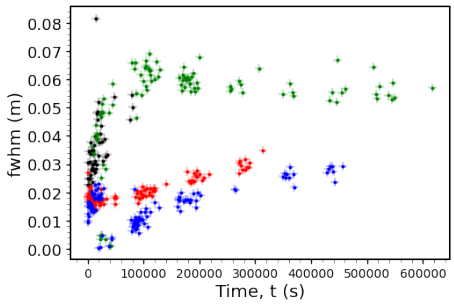

Figure 5: The full width half maximum of the dip in the laser pattern compared to the height of the liquid interface from the data sets as described in table 1 plotted against time.

was found that the general dip shape is asymmetrical and varies for the different solutions and over time. For the Green data, it was observed that the pattern is steepest on the LHS of the dip, closest to the dip, whilst it was the other way round on the RHS; this effect increased with time. For the Red and Black data it was the left and right side were swapped and it decreased over time. For the Blue data it was somewhere in between, starting similar to the Green data, but transitioning into the pattern of the Red & Black.

III.1 Image analysis

An example of the result of the image processing programme is shown in Fig. 6

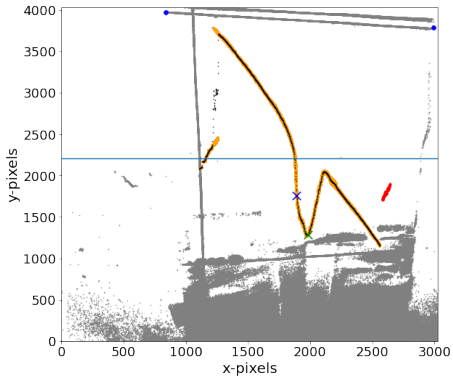

Figure 6: An image of the Blue data set (see table 1). The grey shows the dark pixels in the image, the blue dots show the two reference points used to determine the conversion factor and the reference height. The red shows the laser data but has mostly yellow overlaid as the data used to extract data. The black line in the middle of it shows the average height laser data. The green cross represents the dip found and the blue cross is the point from which the fwhm is determined.

III.2 Modelling

An example of the modelled result is shown in Fig. 7 & 8.

A result that can be drawn from this is that the dip is

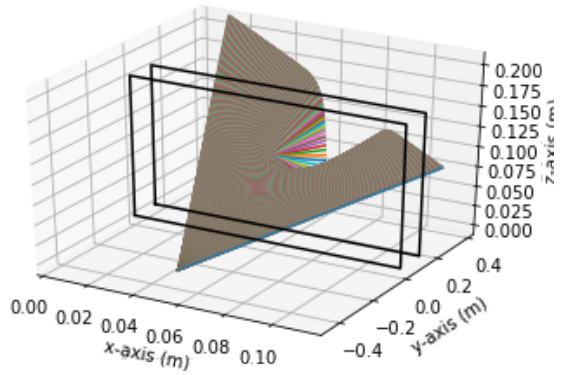

Figure 7: 3D ray-tracing model showing the path on the left from the glass rod, to the container, the edges of which are marked in black, to the screen. The model represents the Red data-set (see table 1) at $t = 4h$ and the temperature T, is 20°C.

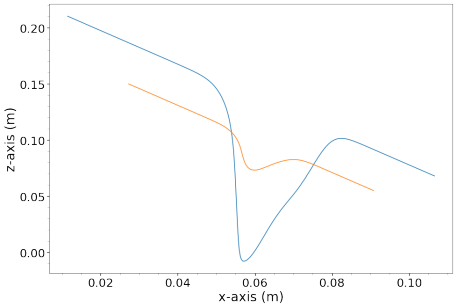

Figure 8: A view along the y-axis at the positions of the light-rays at the end of the container (orange) and on the screen (blue). The rays are those shown in 7

actually not from the light that enters at the liquid interface but instead from the rays that enter a bit above.

IV Discussion

Because of the amplification of errors in point recognition, it was found that transforming the image before extracting data was not sustainable and thus the raw images had to be used. Although this is somewhat compensated for in the conversion factor, the full extent of the length distortion due to the image perspective is not taken into account and provides an unaccounted for error on the data. Additionally, the analysis of the images does not always give the exact right result from the image. This provides an additional error which could not be quantified. It is expected that his has caused the outliers seen in the Black data. This could have been the case for extracting the endpoints of the bottom of the top two horizontal lines, as these were sometimes mixed up by the programme, though not frequently and only for the Black data where these were used.There were also various uncertainties in the set-up itself. Particularly, the approximations having all the equipment at the right height and fully parallel or perpendicular to one-another. For instance, the desk used was observed to be sagging and the cardboard stand used for the laser caused it to move around as one touches it to turn it on. Moreover, given that the set-up was placed on a desk in a bedroom and present for weeks on end, this meant that the fluid inside got disturbed relatively often due to vibrations. This could have an effect on the diffusion.

V Conclusions

Whilst the home-environment caused various inaccuracies in the set-up, the data seem to be consistent with one-another and the dip length converges to a 1/sqrt relationship over longer time. The computational model used seems to accurately represent the optical effect that is observed.

References

[1] J. M. Roussel, M. Gailhanou et al, On the Wiener optical method to study molecular diffusion in liquids, American Journal of Physics 88, 661 (2020).

[2] A. Mordvintsev, Abid K. & OpenCV-Python Tutorials's documentation, Revision 43532856, URL: https://opencv-python-tutroals.readthedocs.io/en/latest/. Accessed on: 07/04/2021.

[3] D. J. Segelstein, The complex refractive index of water, Faculty of the University of Missouri-Kansas City, United States, 1981.

[4] L. F. Hoyt, New Table of the Refractive Index of Pure Glycerol at 20°C, Industrial Engineering Chemistry26 (3), 329-332, 1934.

[5] I. G. Hughes, T. P. A. Hase, Measurements and their Uncertainties, A practical guide to modern error analysis, Oxford university press, New York, United States (2010).

VI Error Appendix

The errors in the measurements made of the set-up were determined to be half the smallest division of the analogue device used. However, this was sometimes increased to the smallest division itself as the parallax was deemed to great. These errors have been propagated according to the Calculus method as detailed in [5]. An error of 2 minutes was taken for the start time of diffusion as no clear starting point could be defined as the diffusion would already start whilst the pouring of the liquids, which takes a few minutes, is still happening. The start time was chosen to be the moment the pouring was finished.

VI.1 Image analysis

VI.1.1 Extracting data

The laser pixels were extracted from the image using a 200 out of 255 minimum for the red and green and blue values set to be lower than the red. Two methods have been employed to find the dip in the laser pattern, if the dip was consistently the lowest point of the entire pattern then it would simply correspond to the minimum value of all the laser data. On the other hand if it was not, then the point was determined by analysing the array of laser data with averaged y-values, being a list of one y-value per x-value. The y-values between subsequent points with a defined interval going from left to right were compared; if the next point went up then the dip would be within that interval. The height of the interface between the two liquids was used as a reference line to determine the length of the dip. From the dimensions measured of this interface to the floor and the paper to the floor the distance from the top corner of the image could be determined. From the distances from the horizontal reference lines (some of which were not ideally parallel to the top of the paper) and how far along the lines the dip is, a projection of this reference line could be made on the paper. The fwhm was found by examining the points which are half the length of the dip above the dip itself and taking twice the distance between whatever outer point was used and the centre. The results of this process can be seen in Fig. 6. The length the top or bottom reference line and the known width of the paper was used as a conversion factor, pixel-distance.

VI.1.2 Automation Diagnosis

With the goal of a fully automated image analysis process all the previous steps had to be made adaptive with (self-)diagnosis. This includes extracting the time the image was taken at from the filename and cycling through all the images in the folder but more importantly changing the parameters which define the above. Firstly, lowering the edge intensity gradient limits if an error occurred in finding the bottom of the 2 horizontal lines at the top of the image or no lines fitted to the laser data could be found. Large $\rho \,\&\, \theta$ intervals were chosen, so no adaptability was required in the actual detection of the lines. Secondly, the pixel RGB intensity limit was determined from the average intensity across the whole image and a changed according to various tests performed on the data. How close the line endpoints found were to the image borders, to an average distance between them found from other images or to endpoints of another line as well as what the result was in a previous run through the loop determined whether the intensity limit should be simply increased, decreased cycled up down around the current value, increasing the jump every time, or whether the image ought to be discarded. Specifically for the vertical reference line, the bottom part of the image was discarded due to shadow present. How much is discarded was changed accordingly and tested by comparing the found endpoint and the height of this limit. Thirdly, different step sizes used in locating the dip were cycled through until a dip was found, which subsequently was adjusted by taking the local minimum again around this dip. Lastly, the right or left side of the dip pattern was used to find the fwhm dependent on where laser data could be extracted. During all these processes diagnoses were exported to show to what extent these parameters had to be changed, which gives an indication of potential invalid data-points.